Applied Catalysis B: Environment and Energy 351 (2024) 123957

Contents lists available at ScienceDirect

Applied Catalysis B: Environment and Energy

journal homepage: www.elsevier.com/locate/apcatb

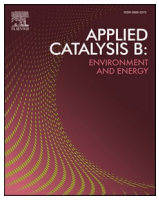

Waste biomass-derived biochar in adsorption-photocatalytic conversion of CO_2 for sustainable energy and environment: Evaluation, mechanism, and life cycle assessment

Xiaoqian Wei [a,b], Xueyang Zhang [c], Li Jin [d], Xianli Yang [a], Weixin Zou [a,*], Bin Gao [b], Lin Dong [a]

[a] State Key Laboratory of Pollution Control and Resource Reuse, School of Environment, School of Chemistry and Chemical Engineering, State Key Laboratory of Coordination Chemistry, Jiangsu Key Laboratory of Vehicle Emissions Control, Nanjing University, Nanjing 210023, PR China
[b] Department of Civil and Environmental Engineering, Rensselaer Polytechnic Institute, Troy, NY 12180, USA
[c] Jiangsu Key Laboratory of Industrial Pollution Control and Resource Reuse, School of Environmental Engineering, Xuzhou University of Technology, Xuzhou 221018, PR China
[d] School of Chemistry, Xi'an Jiaotong University, Xi'an 710049, PR China

ARTICLE INFO

Keywords:
Waste biomass-derived biochar
Adsorption-photocatalytic conversion of CO_2
Ambient conditions
Life-cycle assessment
Mechanism

ABSTRACT

Biochar is an environmentally friendly material with great potential for carbon capture and storage. As the first of its kind, waste biomass-derived biochar was utilized to convert CO_2 into fuel in solar. Herein, among four representatives herbaceous, woody, sludge, and manure wastes, the pine sawdust-derived biochar produced the highest CO assisted by higher CO_2 adsorption, more than 10 times higher than that of graphene and activated carbon. The function groups of carbonyl and carboxyl on biochar controlled the CO_2 capture and solar conversion by decreasing adsorption and activation energies of CO_2 molecules. The biochar performed even better for 15% CO_2/N_2 atmosphere, a typical CO_2 concentration in the flue gas, demonstrating its promising potential in waste gas resource utilization. The life-cycle assessment indicates that feedstock with more cellulose and lignin provide better environmental and economic benefits. The work highlights a sustainability pathway for waste biomass-derived biochar in CO_2-to-fuel under ambient conditions.

1. Introduction

With rapid economic development, bio-waste resources such as agriculture residuals, forestry residuals, industry byproducts, and animal wastes are continuously generated [1]. They are renewable and inexpensive, and thus are ideal feedstock for the production of biochar through pyrolysis in an inert atmosphere [2–4]. Owing to its large specific surface area, well-developed pore structure, high non-carbonized component content, abundant surface functional groups, cost-effectiveness, and sustainability, biochar has been widely applied in the field of energy storage, environmental remediation, catalysis [5–8]. As the CO_2 concentration in the atmosphere has exceeded 410 ppm with a continuous stable increase, carbon capture, storage and utilization (CCSU) become an indispensable need [9,10]. The waste biomass-derived biochar, as porous adsorbent, has attracted much attention in carbon capture to reducing CO_2 emission [9,11,12], but there is little research into their subsequent CO_2 conversion. On the other hand, biochar has excellent electrochemical and catalytic properties [8,13,14], making it a promising agent for CO_2 conversion. It is thus worth of exploring of the application of biochar in CO_2 conversion, which can maximize the benefits of biochar for energy and environmental sustainability.

Comparing CCSU technologies, single adsorption technique involves the risk of secondary pollution, and adsorption-catalytic conversion is typically regarded as a highly efficient method for tackling the problem of CO_2 emissions. Among them, electrocatalysis, photoelectrocatalysis, thermocatalysis and photothermocatalysis possess certain fateful drawbacks, such as high cost and low stability [15]. However, the low-cost solar irradiation has been considered as a sustainable energy to promote CO_2 conversion to produce green and sustainable fuel to solve climate and energy crisis [16]. The functional groups on photocatalysts surface have been verified by numerous studies to strengthen adsorption and activation of CO_2 molecules, reduce the activation energy barrier, thereby speed up the surface catalytic reaction [16–19]. Biochar with

* Corresponding author.
E-mail address: wxzou2016@nju.edu.cn (W. Zou).

https://doi.org/10.1016/j.apcatb.2024.123957
Received 8 January 2024; Received in revised form 1 March 2024; Accepted 13 March 2024
Available online 16 March 2024

multiple functional structures (oxygen-containing groups, persistent free radicals, defects, mineral components, etc.) is promising in the photocatalysis field [20–25]. For example, the dense aromatic structure of biochar can act as an electron shuttle to assist electron migration [26], and the intrinsic oxygenated functional groups are prone to be activated and excited to generate reactive oxygen species (ROS) [22]. In addition, their edge defects with delocalized π-electrons and minerals/organic carbon components are favorable to the reactant adsorption [21,24] and solar light absorption [25], respectively. Therefore, the above excellent characteristics of biochar make them promising catalysts for CO_2 solar conversion.

In the field of catalytic CO_2 conversion, metal-based catalyst materials are most commonly utilized. Zhao's team reported that the prepared metal-based catalysts (i.e., AuZn@ZnO, $Zn^{\delta+}$/ZnO/CeO_2, Cu_2O/ZnO, α-Fe_2O_3/ZnO, etc.) manifested superior photocatalytic activity toward CO_2 conversion [27–31]. However, metal-based catalysts do not have great advantages in terms of cost, corrosion resistance, and stability, limiting their industrial applications [32,33]. Encouragingly, carbon-based materials with low cost and environmental friendliness including graphene, activated carbon, nanofibers, g-C_3N_4, carbon nanotubes and biochar offer certain complementary and emerging applications in catalyzing CO_2 reduction, which are usually in combination with other metallic and nonmetallic composites to enhance CO_2 uptake and conversion [34–36]. In particular, biochar has only been used as supporting materials for metal semiconductors or doped heteroatoms [37–41], which inevitably leads to increased cost and secondary environmental pollution. If biomass-derived pristine biochar can serve as an effective photocatalyst for solar conversion of CO_2 to produce sustainable fuels, it would greatly improve the economic and sustainable viability of CCSU.

Herein, owing to unique characteristics of pine sawdust (PS) with more cellulose, hemicellulose and lignin, wheat straw (WS) with less inorganic compounds, sewage sludge (SS) with more mineral compositions, and cow manure (CM) with less organic compounds, the above four typical biomass wastes were selected as feedstocks for biochar production (Fig. 1A). They were pyrolyzed at relatively low temperatures (300–400 °C) to save energy based on the results of TG (Fig. S1). Furthermore, the waste biomass-derived biochar was applied in CO_2 solar conversion to sustainable fuels without any sacrificial/metal agents or heating conditions. The pine sawdust-derived biochar achieved the best CO fuel production of 39.9 μmol·g^{-1} from CO_2 photoreduction, which was more than 10 times higher than that of other advanced carbon materials (i.e., graphene and activated carbon). Comprehensive characterizations and density functional theory (DFT) calculations revealed the governing mechanism and the role of biochar in CO_2 solar conversion. Moreover, the effect of different CO_2 concentrations in environment and a life-cycle assessment (LCA) of CO fuel product were analyzed in detail to confirm the sustainability benefits. As the first of its kind, this study has opened a door to the potential applications of waste biomass-derived biochar in solar conversion of CO_2 into fuels for sustainable energy and environment.

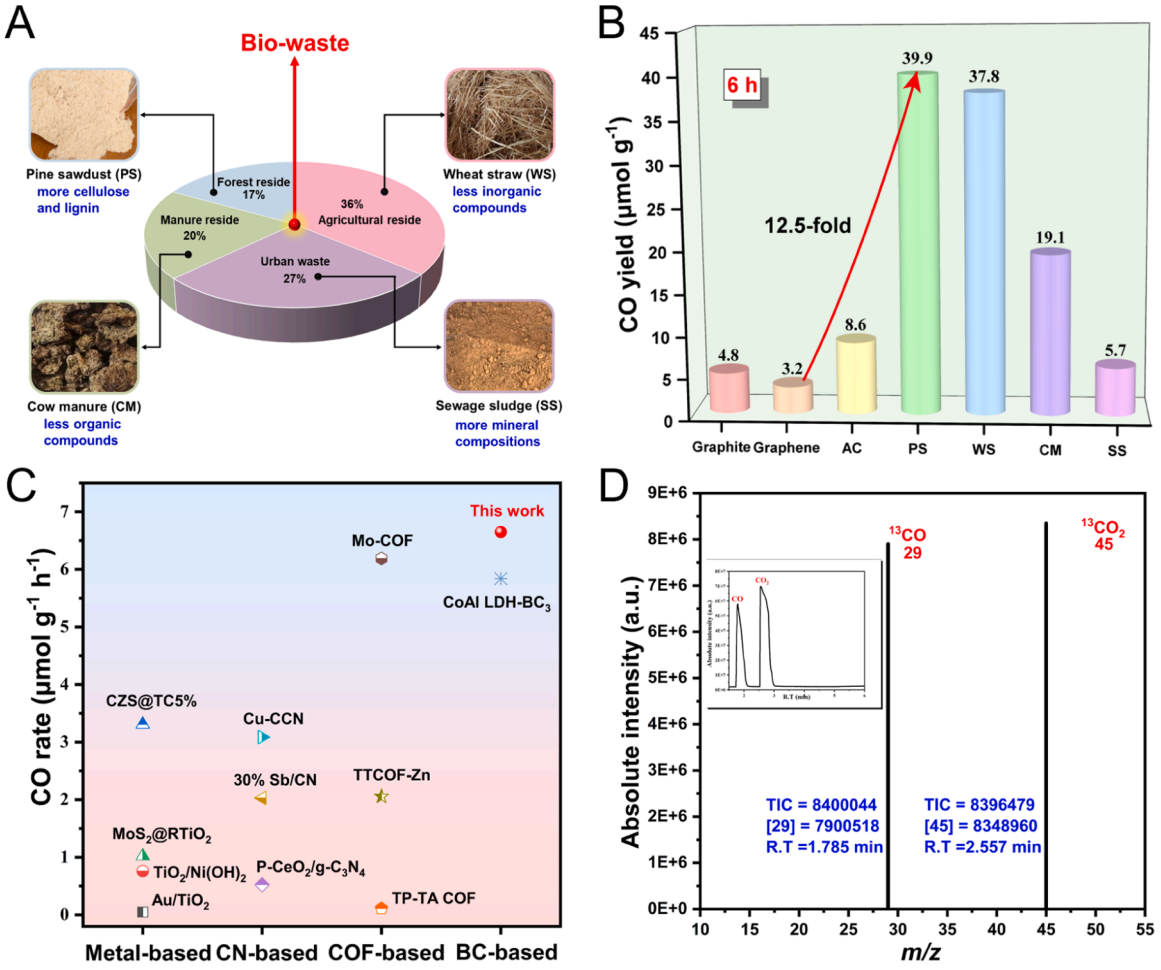

Fig. 1. (A) Composition of four bio-waste resources (based on the data of Wang et al. [47]). (B) Production of CO from CO_2 photoreduction by graphite, graphene, AC, and various waste-derived biochar under light illumination. (C) Comparison of CO evolution rate in solar conversion of CO_2 by PS350 (this work) to that of advanced metal or carbon based photocatalysts in previous studies. (D) GC-MS spectrum of the products of photocatalytic $^{13}CO_2$ reduction over PS350.

2. Materials and methods

2.1. Biochar production

PS, WS, SS, and CM waste biomass obtained from Jiangsu Lianyungang Changyuan straw processing plant, advanced farm, Chemical Baita Industrial Park were selected as the woody, herbaceous, sludge, and livestock manure feedstocks, respectively. The feedstock was ground and passed through 120 mesh sieves, then rinsed with deionized water and oven-dried for future use. For the preparation of biochar, the cleaned biomass powder was pyrolyzed in a tubular furnace (OTF-1200X-II) at a certain temperature with a heating rate of 5 °C/min for 3 h under N_2 atmosphere. The obtained black power was washed using deionized water to remove the impurities and air-dried for 12 h at 100 °C. The product was again dried in the oven at 180 °C for 24 h prior to use. The results of TG (Fig. S1) showed that the pyrolytic zone of the four-biomass ranged from about 200–400 °C, and 350 °C was thus chosen as the pyrolysis temperature to convert the four feedstocks into biochar, which were labeled as PS350, WS350, SS350, and CM350. Three different pyrolysis temperatures (300 °C, 350 °C, and 400 °C) were used to obtained three types of PS biochar (PS300, PS350, and PS400, respectively).

2.2. Characterization

Scanning electron microscopy (SEM) was conducted on an SSX-550 instrument. X-ray powder diffraction (XRD) analysis was operated by a Philips X'Pert Pro diffractometer under Ni-filtered Cu Kα radiation. Fourier transform infrared (FT-IR) spectra were collected from a NICOLET iS10 FT-IR spectrometer. Thermogravimetry analysis (TGA) was taken on a STA 449 C instrument from indoor temperature to 950 °C with a heating rate of 5 °C/min in a purified N_2 atmosphere. N_2 and CO_2 adsorption and desorption isotherms were acquired from the Micrometrics ASAP-2020 device at 77 K and room temperature, respectively. X-ray photoelectron spectroscopy (XPS) data were carried out using a PHI 5000 Versa Probe spectrometer with work function of 4.6 eV and calibrated using the adventitious C 1 s line at 284.6 eV. ^{13}C magic-angle spinning nuclear magnetic resonance (MAS NMR) was measured on a Bruker Avance III spectrometer at 9.4 T and 100.6 MHz. Mineral elements of biochar were detected on an inductive coupled plasma (ICP) emission spectrometer (Avio500). Before the test, the mixture of the sample, nitric acid, hydrogen peroxide, and hydrochloric acid was transferred into a Teflon-lined autoclave and heated at 200 °C for 12 h. The UV–vis diffuse reflectance spectra (DRS) were obtained from a UV-3600 device. The electrochemical impedance spectroscopy (EIS), Mott-Schottky (M-S), and transient photocurrent response experiment were performed on a CHI660E electrochemical workstation with an Ag/AgCl reference electrodes in 0.1 M Na_2SO_4 as electrolyte solution. Boehm titration was used to quantify the surface oxygen-containing functional groups on biochar [42]. The method assumes that sodium ethoxide (C_2H_5ONa) can neutralize carboxylic, lactonic, phenolic hydroxyl, and carbonyl groups; sodium hydroxide (NaOH) can neutralize carboxylic, lactonic, and phenolic hydroxyl groups; sodium carbonate (Na_2CO_3) can neutralize carboxylic, and lactonic groups; sodium bicarbonate ($NaHCO_3$) only neutralizes carboxylic groups. 50 mg of sample was added into 25 mL of 0.05 M C_2H_5ONa, NaOH, Na_2CO_3, $NaHCO_3$, respectively, and shaken for 24 h. The content of various groups was determined by titrating the remaining base with 0.05 mol HCl. In situ diffuse reflectance infrared Fourier transform spectra (DRIFTS) for the adsorption and photocatalytic reduction processes of CO_2 and H_2O were recorded with a Nicolet Nexus 5700 FTIR spectrometer. The sample was filled into the infrared cell and pretreated at 200 °C in purified N_2 for 1 h, then kept to 30 °C. Thereafter, water vapor is brought into the reaction cell in the form of a bubble of CO_2 gas (pure CO_2 and 15% CO_2/N_2). The adsorption and photocatalytic DRIFTS data were collected for 1 h in dark and under the 280 W Xe lamp irradiation, respectively.

2.3. Computational methodology

Different oxygen-containing functional groups (carboxyl, carbonyl, hydroxyl, and lactones groups) by grafting or substituting C and H atoms are constructed on the edges of coronene that was chosen as the basic structure of the carbonaceous skeleton of the biochar, which is an acknowledged model reported previously in the literature [43]. Theoretical models were exploited to calculate its adsorption and activation capability for CO_2. The calculations in this work are performed using the DMol3 scheme [44], which is fully optimized based on DFT calculations. Perdew-Burke-Ernzerhof (PBE) functional in the generalized gradient approximation (GGA) was chosen to describe the exchange correlation potential [45]. The Tkatchenko and Scheffler (TS) scheme was used to correct for the influence of van der Waals (vdW) forces [46]. The total energy was set to 1×10^{-5} Ha (Hartree) with $1\times1\times1$ Monkhorst-pack k-points grid. The tolerance of residual force was set as 0.002 Ha/Å. The maximum displacement below 0.005 Å was set as the convergence thresholds in geometry optimization.

2.4. Evaluation of photocatalytic CO_2 reduction

The photocatalytic CO_2 reduction was tested in a closed system under 280 W Xe lamp irradiation. Specifically, 10 mg of BC samples were added into 1 mL of deionized water and ultrasounded for 0.5 h, then uniformly dispersed on a quartz sand plate ware with a diameter of 4.2 cm, placed in a 100 mL stainless steel reactor. High purity CO_2 or 15% CO_2/N_2 was filled into the reactor up to 0.2 MPa and irradiated for 6 h after dark treatment for 1 h. The product CO was detected and analyzed by online gas chromatography (GC-7920) periodically (1 h). The CO yield (Y_{CO}) was calculated by the following formula:

$$Y_{CO} = \frac{A_t[CO]_s P_r V_r}{A_s R T_r m_{cat.}}$$

where A_t is the peak area of CO at time t; A_s and $[CO]_s$ represent peak area and concentration (ppm) of the CO standard gas, respectively; R is molar gas constant; P_r, V_r, and T_r are the pressure, gas volume, and temperature inside the reactor, respective; $m_{cat.}$ is the mass of the photocatalyst biochar.

3. Results and discussion

3.1. Adsorption-photocatalytic conversion CO_2-to-CO

The waste biomass-derived pristine biochar prepared at 350 °C were used in the reaction of CO_2 conversion by solar with full-spectrum without the addition of any metals or sacrificial agents, or heating. All four biochar demonstrated the ability of solar conversion of CO_2 to CO fuel, and PS-derived biochar exhibited the highest CO production of 39.9 $\mu mol\cdot g^{-1}$ in 6 h with the assistance of higher CO_2 adsorption capacity (Fig. S2), which was about 13 and 5 times higher than that of graphene and activated carbon (AC), respectively (Fig. 1B). Particularly, in comparison to previous studied metal and carbon-based advanced materials (e.g., g-C_3N_4 (CN), COF, and biochar (BC)), the waste biomass-derived biochar performed much better in the solar conversion of CO_2 to CO (Fig. 1C and Table S1). Even under the normal pressure (NP) reaction conditions, the PS350 can still display a favorable CO generation yield in 6 h (28.4 $\mu mol\cdot g^{-1}$, Fig. S3). What's more, no significant decay was observed in the CO yield of PS350 catalyst in cycle tests (Fig. S4), highlighting its superior stability and practical application potential. In order to confirm the CO fuel was a product from CO_2 instead of biochar, $^{13}CO_2$ was used in the solar conversion experiment to trace the product source (Fig. 1D). In the GC-MS spectrum, peaks at m/z = 45 and 29 correspond to the fragments of $^{13}CO_2$ and ^{13}CO, respectively. This confirmed the exclusive formation of the evolved CO from the reduction of CO_2, rather than from the decomposition of the biochar. Therefore,

waste biomass-derived biochar is an effective and sustainable catalyst for solar conversion of CO_2.

3.2. Mechanism exploration

The unique catalytic performances of biochar are often ascribed to their mineral elements and functional groups, and mineral elements are closely related to the biomass feedstocks. Herein, in four biochar samples of PS, WS, CM and SS at different pyrolysis temperatures (300 °C, 350 °C, 400 °C), their main mineral elements of Al, Fe, Mg, Ca, Mn, P, Si, Na, K were determined by the ICP method (Table S2). The corresponding relationships between the mineral elements and CO yield are shown in Figs. 2 and S5. After a simple correlation analysis with Pearson's product-moment correlation coefficient (r), it was observed that there were no positive correlations between mineral elements and CO yields from CO_2 reduction ($r = -0.43$, $R^2 = 0.18$, Fig. 2A), revealing that not all of biochar's functional structures, i.e., mineral components, exhibit catalytic activity for CO_2 conversion. The weak negative correlation ($0 \leq R^2 < 0.3$) phenomenon presented by the CO generation from CO_2 reduction and mineral elements contributions may be attributed to the increase in surface polarity induced by endogenous minerals in the biochar inhibiting the adsorption and activation of CO_2 and H_2O molecules [48]. Among these elements, Al ($r_{Al} = -0.89$, $R^2_{Al} = 0.79$, Fig. 2B-C) and Fe ($r_{Fe} = -0.87$, $R^2_{Fe} = 0.76$, Fig. 2B and D) even presented strong negative correlations with the CO_2-to-CO rate. For the rest of the elements of Mg, Ca, Mn, P, Si, Na, K in the ash, there were no significant correlation ($R^2 < 0.5$) with the CO_2-to-CO rate (Figs. 2B and S5A-G). Interestingly, the correlations between mineral elements and CO_2 adsorption capacity (Fig. S5H) are highly consistent with CO yields, which is attributed to the fact that except for Al and Fe elements in the form of sulfate, the rest of main mineral elements are existed in the forms of carbonates, bicarbonates, or chlorides in the ash of biochar, and the high content of soot particles would block the pores and occupy the adsorption sites of biochar, which are not conducive to CO_2 adsorption and reduction, reducing biochar's ability for CO_2 solar conversion [49–51]. These results indicate that metal elements in the waste biomass-derived biochar were not the important factors for solar conversion of CO_2.

Biochar's oxygen containing function groups are usually affected by the pyrolysis temperatures, and the PS-derived biochar prepared at different temperatures (i.e., PS300, PS350, and PS400) were used to investigate the relationship between function groups and CO fuel yield. All three PS-derived biochar samples exhibited the similar shapes (Fig. S6) and specific surface areas (Fig. S7). The band structures were examined by Mott-Schottky and valence band (VB) XPS methods (Figs. S8–11), showing that all the conduction bands (CB) of PS300 (-1.03 eV), PS350 (-1.06 eV), and PS400 (-1.01 eV) were more negative than the standard reduction potential of CO_2-to-CO (-0.53 eV) [52]. Therefore, they can thermodynamically convert CO_2 to CO (Fig. S12) following the order of PS350 > PS300 > PS400. Moreover, the XRD patterns (Fig. S13) and FT-IR spectra (Fig. S14, Table S3) suggested that with the increased carbonization temperature, the surface functional groups of biochar decreased but the aromaticity enhanced [53]. The XPS and Boehm titration techniques were combined to ascertain the

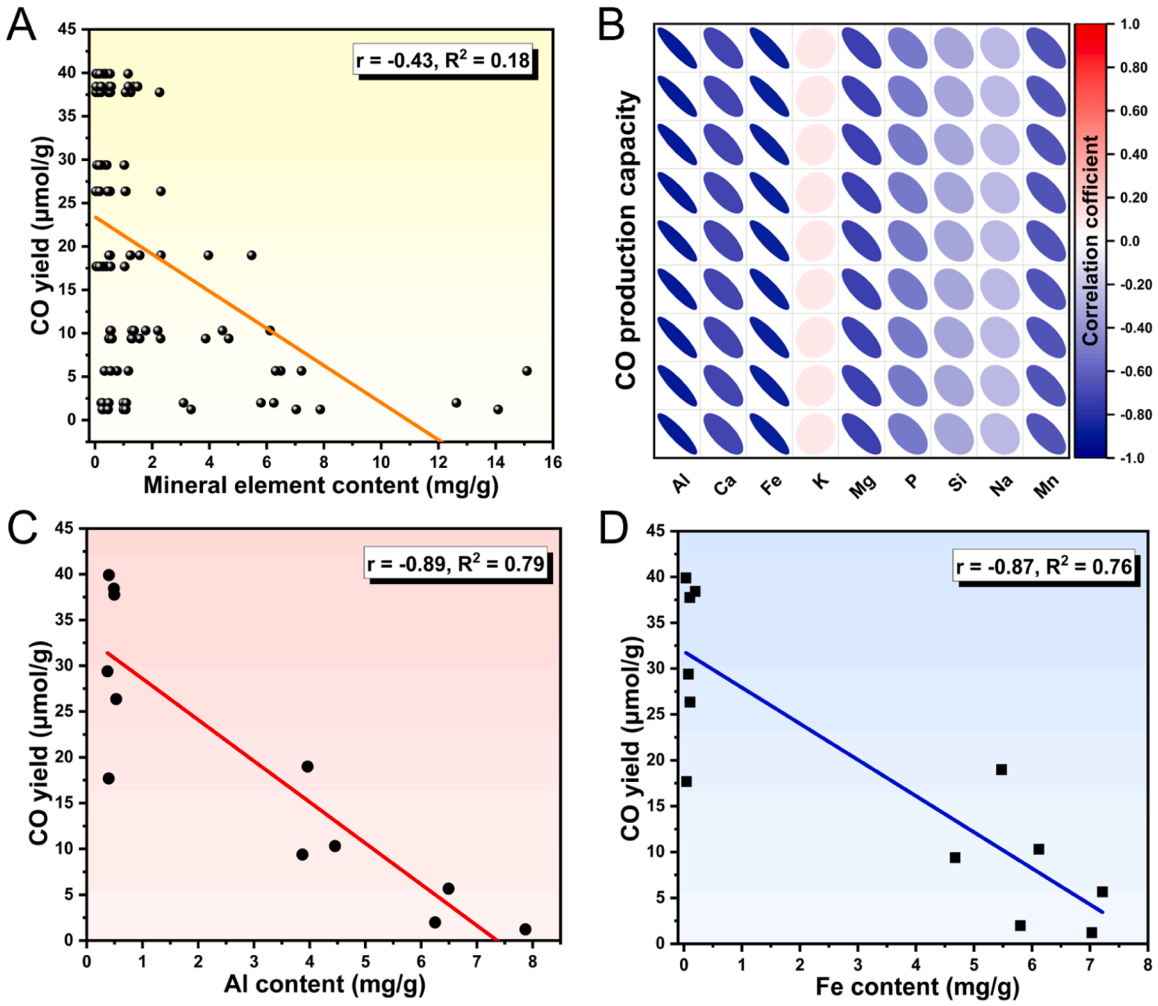

Fig. 2. Relationships between (A-B) all, (C) Al, (D) Fe mineral elements of biochar and CO yields from photocatalytic CO_2 conversion.

qualitative and quantitative information of functional groups of biochar. In high-resolution XPS spectra of C 1 s illustrated in Fig. S15A, three characteristic peaks centered at about 288.7, 286.2, and 284.6 eV can be ascribed to O-C═O, C-O, and C-C/C═C groups, respectively [54]. The O 1 s spectra (Fig. S15B) were fitted into three peaks with the binding energy values of 533.7 eV (H_2O/-OH), 532.9 eV (C═O), and 531.7 eV (C-OH/C-O-C) [55,56]. The details on the relative concentrations of the different types of groups are shown in Table S4 and Fig. 3A. In comparison to PS300 (37.49%, 4.74%) and PS400 (31.26%, 5.05%), PS350 (39.87%, 6.02%) had more C═O and O-C═O. In addition, the Boehm titration data (Fig. 3B) confirmed that the presence of a larger amount of carboxyl (-COOH) and carbonyl (C═O) groups in PS350 sample. Furthermore, the ^{13}C NMR results of the PS350 samples before and after the photoreduction CO_2 reaction were measured (Fig. 3C and Table S5). The used PS350 sample displayed similar peaks as the fresh PS350, suggesting that the PS350 biochar was stable during the photocatalytic reaction. Interestingly, the relative intensities of the -COOH (178 ppm) and C═O (198 ppm) to others became weaker after the reaction [57, 58], suggesting that -COOH and C═O groups could act as the key reaction sites for the solar conversion of CO_2 to CO fuel.

The DFT calculation was carried out to validate the key role of function groups in CO_2-to-CO fuel, and the adsorption conformations and energies were calculated (Figs. S16–17 and Table S6). Unlike other functional groups, -COOH group preferred to interact with O atom (CO_2 molecule) via the hydrogen bonds, exhibiting a smaller minimum adsorption distance (2.14 Å) than C═O group (2.94 Å). On the other hand, the p-electrons of O atom (C═O group) as Lewis base interacted with electron-deficient C atom (CO_2). Therefore, under the above interactions of hydrogen bonds and p-electrons, the bond polarization of CO_2 molecule was enhanced, leading to its activation, break, and reduction. Because of the lower adsorption energies of CO_2 on -COOH (-0.197 eV) than that on C═O (-0.346 eV) groups, the rate-determining step in CO_2 conversion was the generation of key *COOH intermediate. Furthermore, in situ DRIFTS of CO_2 adsorption was performed to explore the CO_2 activation on PS350. As depicted in Fig. 4A, once CO_2 reactant was applied, the peak (1538 cm^{-1}) corresponding to the monodentate carbonate species (m-CO_3^{2-}) appeared [59]. Subsequently, the band (1706 cm^{-1}) related to *COO species generated [57], due to the stronger interaction between p-electrons of O atom (C═O group) and C atom (CO_2). All these are consistent with the DFT results. Afterward, the formation of HCO_3^- species (1648 cm^{-1}) was attributed to the synergistic interactions of hydrogen bonds (-COOH group) and p-electrons (C═O group) for CO_2 activation and reduction [60]. Therefore, PS350 biochar with the most abundant carbonyl and carboxyl groups exhibited the best ability of CO_2 solar conversion. Whereas, on PS300 (Fig. S18A), the peak intensities of intermediates were weaker than that of PS350, suggesting

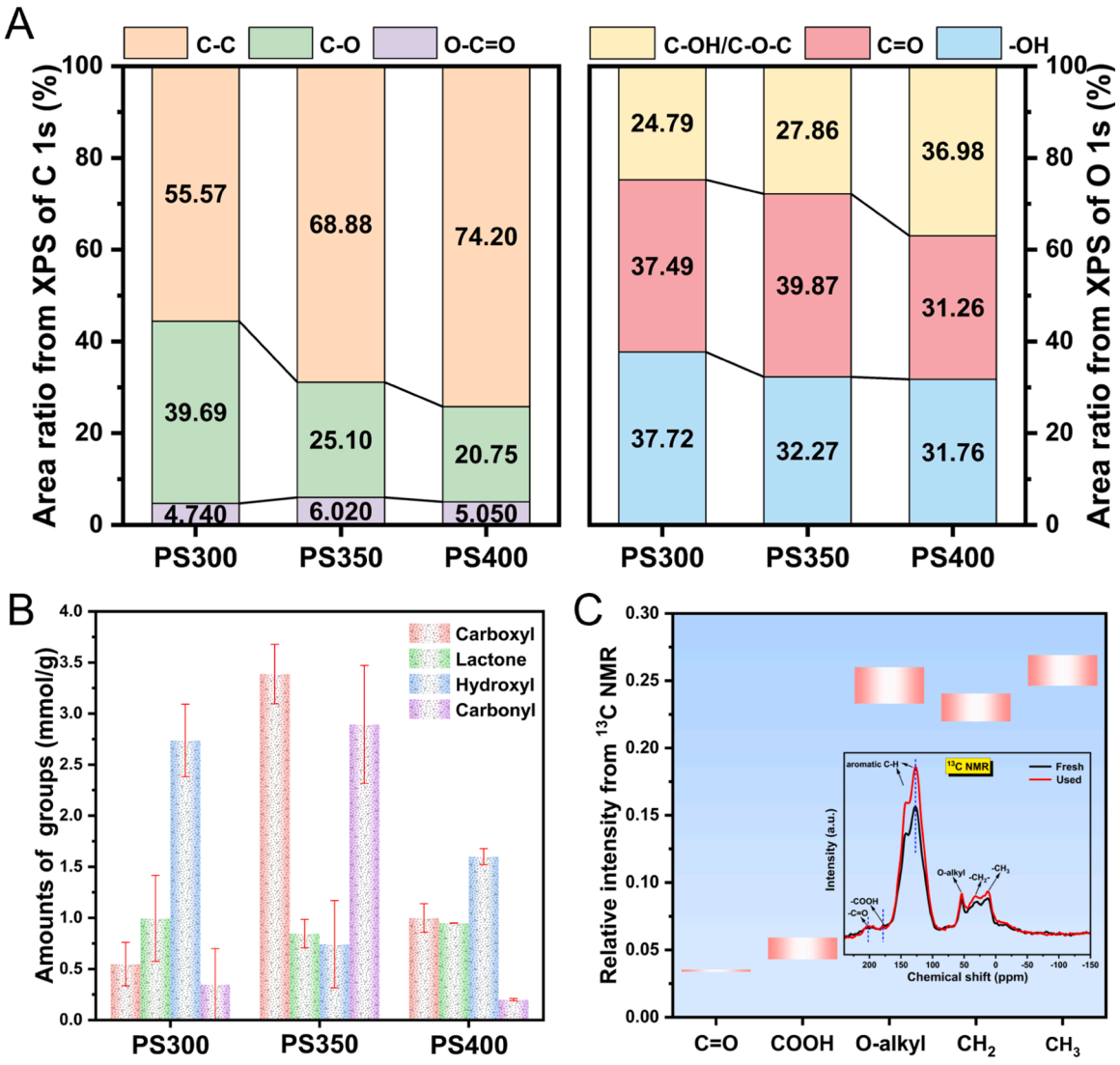

Fig. 3. (A) Area ratio plots from XPS of C 1 s and O 1 s. (B) Contents of various functional groups from Boehm titration of PS300, PS350, and PS400. (C) Change of group content of PS350 before and after photocatalytic CO_2 reduction (inset: ^{13}C MAS NMR spectra of PS350 before and after).

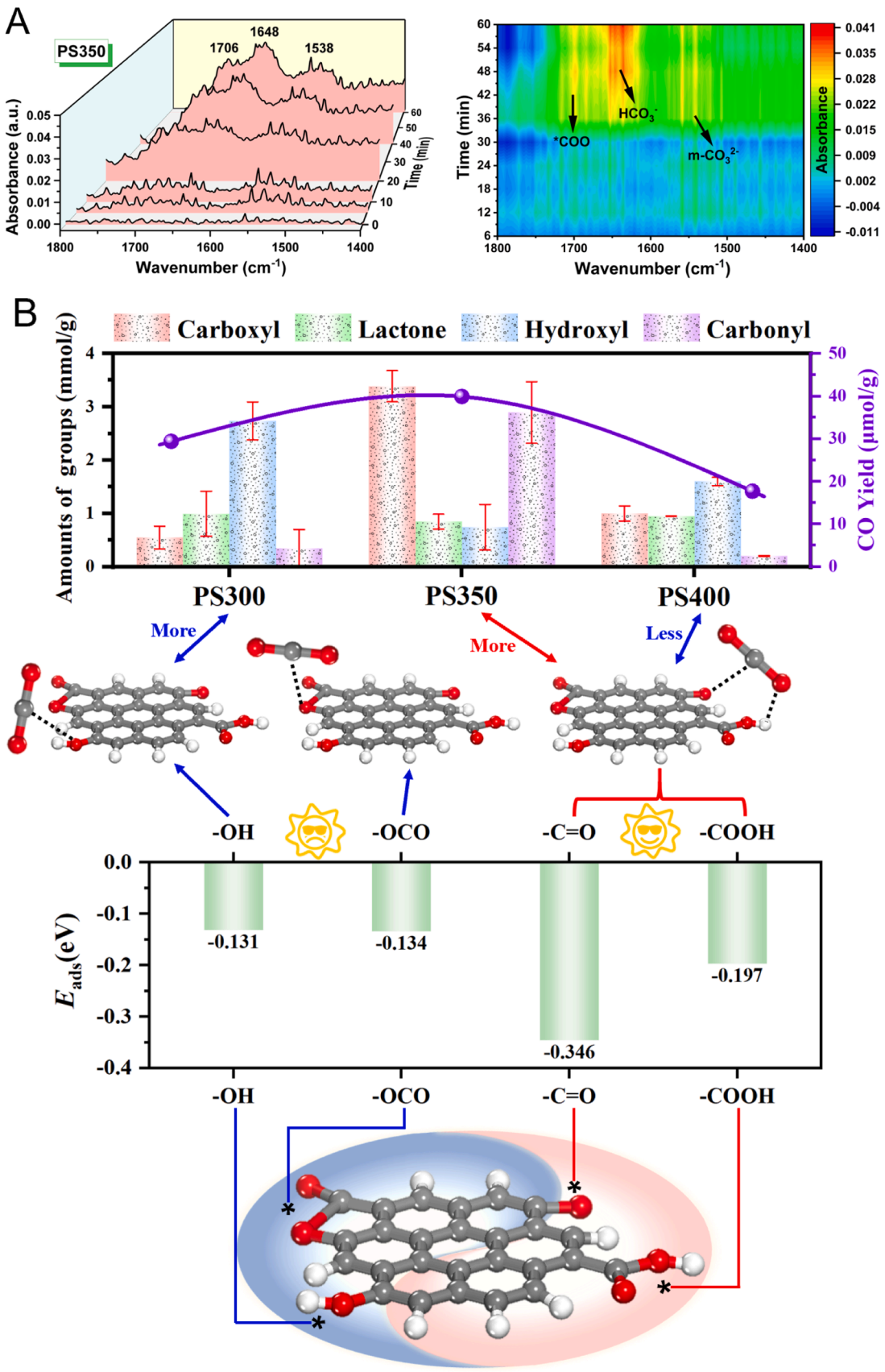

Fig. 4. (A) In situ DRIFTS of pure CO_2 and H_2O vapor co-adsorption on PS350 within 60 min at 30 °C in dark. (B) Schematics of the mechanism for CO_2 activation by different oxygen-containing functional groups on biochar.

that the phenolic hydroxyl groups on the PS300 surface were undesirable for the adsorption and activation of CO_2. This is also consistent with the DFT calculations. For PS400 sample (Fig. S18B), only two weak peaks of *COO and m-CO_3^{2-} species were observed, too few to activate CO_2 for the solar conversion.

On the basis of the qualitative and quantitative results of functional groups, the DFT calculations, and in situ characterizations, the governing mechanism of biochar enabled solar conversion of CO_2 can be determined as follows. Owing to PS350's abundant carbonyl (C═O) and carboxyl (-COOH) groups, the bonds of CO_2 reactant could be activated and polarization, through the synergistic interactions of hydrogen bonds (-COOH group) and p-electrons (C═O group), leading to the subsequent solar conversion to CO fuel. Whereas more phenolic hydroxyl groups on the PS300 surface and fewer carboxyl groups on PS400 were poorer for CO_2 adsorption and conversion (Fig. 4B). In comparison with published studies on carbon-based materials supplied in Table S7, we identified

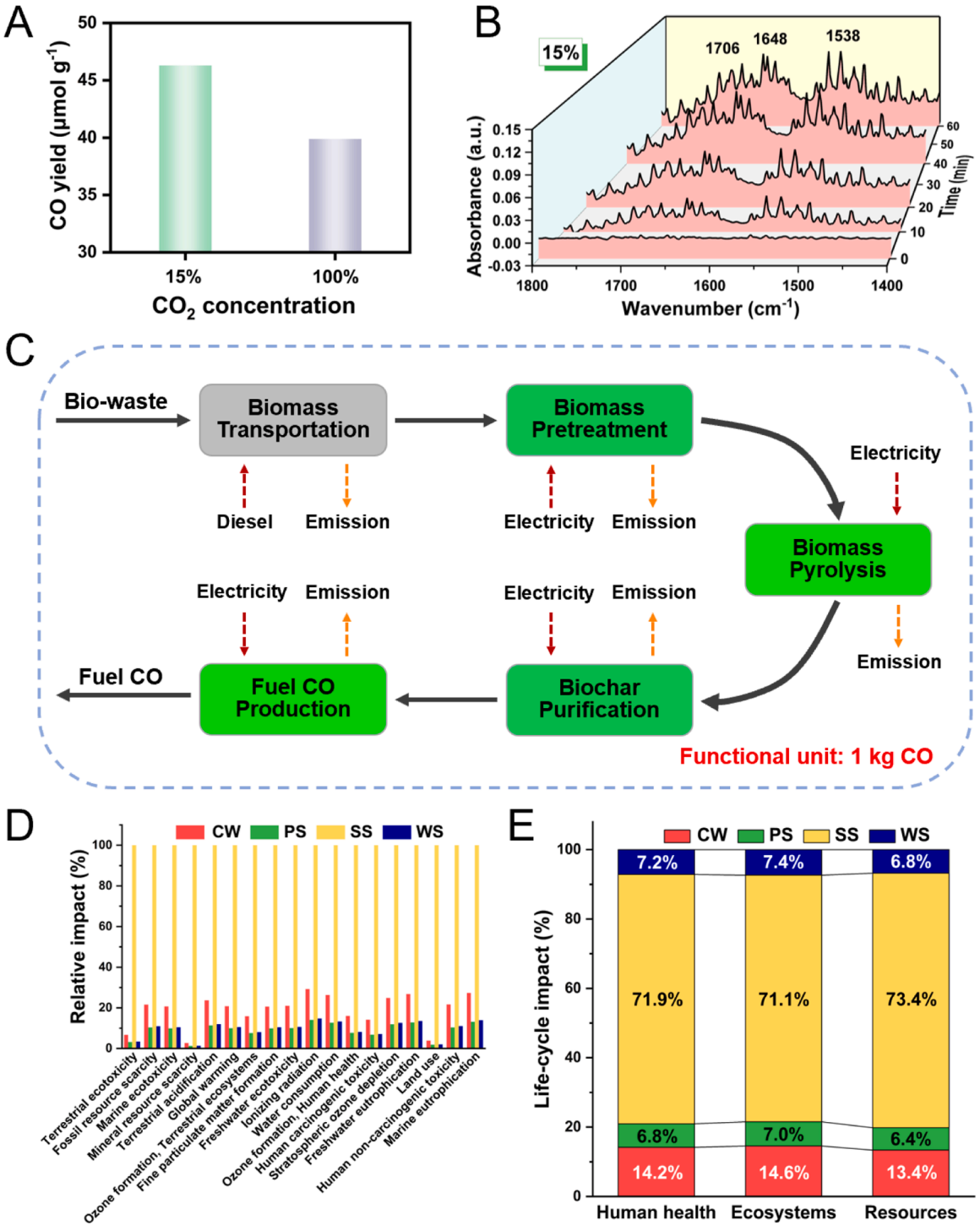

Fig. 5. (A) Production of CO on PS350 biochar for photocatalytic conversion of CO_2 of different concentrations. (B) In situ DRIFTS of adsorption of 15% CO_2/N_2 on PS350 in the presence of H_2O within 60 min at 30 °C. (C) System boundary of life cycle assessment for production of fuel CO from solar conversion of CO_2 by biochar. Comparison of LCIA (D) characterization and (E) normalized aggregated results by ReCiPe 2016 Midpoint (H)/World (2010) H and ReCiPe 2016 Endpoint (H)/World (2010) H/A methods.

specific key oxygen-containing functional groups as well as interaction mechanism.

3.3. Practical application and life cycle assessment

Since environmental systems of pure CO_2 are barely existent in practice, 15% CO_2/N_2, as the typical CO_2 concentrations in flue gas, was selected to examine the application of biochar in solar conversion of CO_2. As shown in Figs. 5A and S19, the yield of CO increased under the condition of 15% CO_2/N_2 (46.3 μmol·g^{-1}), even higher than that under the pure CO_2 condition, indicating promising prospective of the biochar in waste gas resource utilization. In situ DRIFTS of adsorption in different reaction atmospheres of pure CO_2 and 15% CO_2/N_2 were carried out (Figs. 4A and 5B). The peak intensities of the key *COOH and HCO_3^- intermediates in the flue gas of 15% CO_2/N_2 were more intensive than that in the gas environment of pure CO_2, suggesting that the lower CO_2 concentration was beneficial for the adsorption and activation, resulting in the more effective conversion of CO_2 to fuel. These results confirm that waste biomass-derived biochar have promising applications in utilization CO_2 in the industrial flue gas under practical conditions.

In order to further evaluate the sustainability of waste biomass-derived biochar for CO_2 solar conversion, a life cycle assessment (LCA) was conducted to quantify the environmental impact and contribution of the process for CO fuel production from CO_2. Waste biomass-to-CO fuel (cradle-to-gate) and 1 kg of CO product were defined as the system boundary and functional unit in the analysis, respectively (Fig. 5C). The inventory of inputs and outputs for the whole product life cycle is summarized in Table S8, where the data were obtained from databases, literature, calculations, and experiments, etc. Next, the environmental impacts in the process of CO fuel production from CO_2 by different waste biomass-derived biochar (including 18 impact indicators, Table S9) were quantitatively analyzed based on the ReCiPe 2016 Midpoint (H)/World (2010) H methodology [3,61]. Based on 18 midpoint categories, the photoconversion of CO_2 on biochar from low-temperature pyrolysis of PS and WS biomass exhibited considerable environmental superiority, followed by CW, while SS showed the environmental unfriendliness (Fig. 5D). We normalized and aggregated the results of 22 impact categories calculated with the ReCiPe 2016 Endpoint (H)/World (2010) H method (Table S10) to three higher-level LCIA impact indicators of human health, ecosystems, and resources [3, 61]. According to the normalized aggregated results (Table S11 and Fig. 5E), the CO fuel production system from PS and WS showed lower environmental footprint than that from CM and SS. Taken together, the selection of waste biomass with more cellulose and lignin as precursors for biochar was more conducive to achieving efficient CO_2 conversion and environmental benefits.

4. Conclusion

Waste biomass-derived biochar were prepared from woody, herbaceous, chemical sludge, and livestock manure with different characteristics at relatively low pyrolysis temperatures. The biochar was applied in solar conversion of CO_2 to high-value CO fuel. The pine sawdust-derived biochar with rich carbonyl functional groups yielded the highest CO fuel with the aid of greater CO_2 adsorption capacity, in the absence of any sacrificial, metal agents, or heating. It performed even more excellent in 15% CO_2/N_2, a typical CO_2 concentration in the industrial flue gas. Furthermore, the life-cycle assessment revealed that the biochar derived from biomass with more cellulose and lignin exhibited higher CO_2 conversion and environmental benefits. This work provides a new breakthrough on the application of biomass waste-derived biochar in high efficiency solar conversion of CO_2 for sustainable energy and environment.

CRediT authorship contribution statement

Xueyang Zhang: Validation, Resources, Methodology. **Li Jin:** Validation, Methodology. **Xianli Yang:** Resources, Methodology. **Weixin Zou:** Writing – review & editing, Supervision, Funding acquisition, Conceptualization. **Xiaoqian Wei:** Writing – original draft, Validation, Software, Methodology, Investigation, Data curation. **Lin Dong:** Writing – review & editing, Supervision, Funding acquisition, Conceptualization. **Bin Gao:** Writing – review & editing, Supervision, Conceptualization.

Declaration of Competing Interest

The authors declare that they have no known competing financial interests or personal relationships that could have appeared to influence the work reported in this paper.

Data availability

Data will be made available on request.

Acknowledgments

W.Z. and L.D. would like to acknowledge the support of the National Natural Science Foundation of China (62375120, 21972062).

Appendix A. Supporting information

Supplementary data associated with this article can be found in the online version at doi:10.1016/j.apcatb.2024.123957.

References

[1] T. Shan, Y. Li, S. Ke, B. Su, L. Shen, S. Wang, X. Yang, M. Yang, An embedded ReS_2@$MAPbBr_3$ heterostructure with downhill interfacial charge transfer for photocatalytic upgrading of biomass-derived alcohols to aldehydes and H_2, J. Mater. Sci. Technol. 179 (2024) 155–165.
[2] S. Sohi, Carbon storage with benefits, Science 338 (2012) 1034–1035.
[3] S. Zhang, S. Jiang, B. Huang, X. Shen, W. Chen, T. Zhou, H. Cheng, B. Cheng, C. Wu, W. Li, H. Jiang, H. Yu, Sustainable production of value-added carbon nanomaterials from biomass pyrolysis, Nat. Sustain. 3 (2020) 753–760.
[4] W. Liu, W. Li, H. Jiang, H. Yu, Fates of chemical elements in biomass during its pyrolysis, Chem. Rev. 117 (2017) 6367–6398.
[5] W. Liu, H. Jiang, H. Yu, Development of biochar-based functional materials: toward a sustainable platform carbon material, Chem. Rev. 115 (2015) 12251–12285.
[6] S. Li, X. Han, W. Song, Z. Wang, Y. Zhu, S. Jiao, Nickel-promoted electrocatalytic graphitization of biochars for energy storage: mechanistic understanding using multi-scale approaches, Angew. Chem. Int. Ed. 62 (2023) e202301985.
[7] Z. Weng, L. Zwieten, E. Tavakkoli, M. Rose, B. Singh, S. Joseph, L. Macdonald, S. Kimber, S. Morris, T. Rose, B. Archanjo, C. Tang, A. Franks, H. Diao, S. Schweizer, M. Tobin, A. Klein, J. Vongsvivut, S. Chang, P. Kopittke, A. Cowie, Microspectroscopic visualization of how biochar lifts the soil organic carbon ceiling, Nat. Commun. 13 (2022) 5177.
[8] M. He, Z. Xu, D. Hou, B. Gao, X. Cao, Y. Ok, J. Rinklebe, N. Bolan, D. Tsang, Waste-derived biochar for water pollution control and sustainable development, Nat. Rev. Earth Environ. 3 (2022) 444–460.
[9] X. Yuan, M. Suvarna, S. Low, P. Dissanayake, K. Lee, J. Li, X. Wang, Y. Ok, Applied machine learning for prediction of CO_2 adsorption on biomass waste-derived porous carbons, Environ. Sci. Technol. 55 (2021) 11925–11936.
[10] J. Wang, Z. Li, Z. Luo, Y. Huang, F. Ma, S. Kupfer, G. Ouyang, Boosting CO_2 photoreduction by π-π-induced preassembly between a Cu(I) sensitizer and a pyrene-appended Co(II) catalyst, Proc. Natl. Acad. Sci. USA 120 (2023) e2221219120.
[11] J. Moorea, S. Jevrejevad, A. Grinstede, Efficacy of geoengineering to limit 21st century sea-level rise, Proc. Natl. Acad. Sci. USA 107 (2010) 15699–15703.
[12] P. Dissanayake, S. Choi, A. Igalavithana, X. Yang, D. Tsang, C. Wang, H. Kua, K. Lee, Y. Ok, Sustainable gasification biochar as a high efficiency adsorbent for CO_2 capture: a facile method to designer biochar fabrication, Renew. Sustain. Energy Rev. 124 (2020) 109785.
[13] S. Wang, P. Liao, L. Cen, H. Cheng, Q. Liu, Biochar promotes arsenopyrite weathering in simulated alkaline soils: electrochemical mechanism and environmental implications, Environ. Sci. Technol. 57 (2023) 8373–8384.
[14] J. Qu, Z. Li, F. Bi, X. Zhang, B. Zhang, K. Li, S. Wang, M. Sun, J. Ma, Y. Zhang, A multiple Kirkendall strategy for converting nanosized zero-valent iron to highly

active Fenton-like catalyst for organics degradation, Proc. Natl. Acad. Sci. USA 120 (2023) e2304552120.
[15] G. Yergaziyeva, Z. Kuspanov, M. Mambetova, N. Khudaibergenov, N. Makayeva, C. Daulbayev, Advancements in catalytic, photocatalytic, and electrocatalytic CO_2 conversion processes: current trends and future outlook, J. CO2 Util. 80 (2024) 102682.
[16] B. Su, Y. Kong, S. Wang, S. Zuo, W. Lin, Y. Fang, Y. Hou, G. Zhang, H. Zhang, X. Wang, Hydroxyl-bonded Ru on metallic TiN surface catalyzing CO_2 reduction with H_2O by infrared light, J. Am. Chem. Soc. 145 (2023) 27415–27423.
[17] B. Su, M. Zheng, W. Lin, X. Lu, D. Luan, S. Wang, X. Lou, S-scheme Co_9S_8@ $Cd_{0.8}Zn_{0.2}S$-DETA hierarchical nanocages bearing organic CO_2 activators for photocatalytic syngas production, Adv. Energy Mater. 13 (2023) 2203290.
[18] G. Chen, Z. Zhou, B. Li, X. Lin, C. Yang, Y. Fang, W. Lin, Y. Hou, G. Zhang, S. Wang, S-scheme heterojunction of crystalline carbon nitride nanosheets and ultrafine WO_3 nanoparticles for photocatalytic CO_2 reduction, J. Environ. Sci. 140 (2024) 103–112.
[19] S. Barman, A. Singh, F. Rahimi, T. Maji, Metal-free catalysis: a redox-active donor-acceptor conjugated microporous polymer for selective visible-light-driven CO_2 reduction to CH_4, J. Am. Chem. Soc. 143 (2021) 16284–16292.
[20] X. He, N. Zheng, R. Hu, Z. Hu, J. Yu, Hydrothermal and pyrolytic conversion of biomasses into catalysts for advanced oxidation treatments, Adv. Funct. Mater. 31 (2021) 2006505.
[21] X. Zhou, Y. Zhu, Q. Niu, G. Zeng, C. Lai, S. Liu, D. Huang, L. Qin, X. Liu, B. Li, H. Yi, Y. Fu, L. Li, M. Zhang, C. Zhou, J. Liu, New notion of biochar: a review on the mechanism of biochar applications in advanced oxidation processes, Chem. Eng. J. 416 (2021) 129027.
[22] I. Velo-Gala, J. López-Peñalver, M. Sánchez-Polo, J. Rivera-Utrilla, Role of activated carbon surface chemistry in its photocatalytic activity and the generation of oxidant radicals under UV or solar radiation, Appl. Catal. B Environ. 207 (2017) 412–423.
[23] G. Fang, C. Liu, Y. Wang, D. Dionysiou, D. Zhou, Photogeneration of reactive oxygen species from biochar suspension for diethyl phthalate degradation, Appl. Catal. B Environ. 214 (2017) 34–45.
[24] X. Cheng, H. Guo, Y. Zhang, G. Korshin, B. Yang, Insights into the mechanism of nonradical reactions of persulfate activated by carbon nanotubes: activation performance and structure-function relationship, Water Res. 157 (2019) 406–414.
[25] H. Shi, M. Wang, B. Wang, Q. Huang, S. Gao, Insights on photochemical activities of organic components and minerals in dissolved state biochar in the degradation of atorvastatin in aqueous solution, J. Hazard. Mater. 392 (2020) 122277.
[26] Y. Zhai, Y. Dai, J. Guo, L. Zhou, M. Chen, H. Yang, L. Peng, Novel biochar@ $CoFe_2O_4/Ag_3PO_4$ photocatalysts for highly efficient degradation of bisphenol a under visible-light irradiation, J. Colloid Interface Sci. 560 (2020) 111–121.
[27] R. Zhao, Z. Zhu, T. Ouyang, Z. Liu, Selective CO_2-to-syngas conversion enabled by bimetallic gold/zinc sites in partially reduced gold/zinc oxide arrays, Angew. Chem. Int. Ed. 63 (2024) e202313597.
[28] S. Guo, Y. Du, H. Luo, Z. Zhu, T. Ouyang, Z. Liu, Stabilizing undercoordinated Zn active sites through confinement in CeO_2 nanotubes for efficient electrochemical CO_2 reduction, Angew. Chem. Int. Ed. 63 (2024) e202314099.
[29] S. Du, P. Yang, M. Li, L. Tao, S. Wang, Z. Liu, Catalysts and electrolyzers for the electrochemical CO_2 reduction reaction: from laboratory to industrial applications, Chem. Commun. 60 (2024) 1207.
[30] S. Guo, Z. Tang, Y. Du, T. Liu, T. Ouyang, Z. Liu, Chlorine anion stabilized Cu_2O/ ZnO photocathode for selective CO_2 reduction to CH_4, Appl. Catal. B Environ. 321 (2023) 122035.
[31] T. Ouyang, Y. Ye, C. Tan, S. Guo, S. Huang, R. Zhao, S. Zhao, Z. Liu, 1D α-Fe_2O_3/ ZnO junction arrays modified by Bi as photocathode: high efficiency in photoelectrochemical reduction of CO_2 to HCOOH, J. Phys. Chem. Lett. 13 (2022) 6867–6874.
[32] Y. Wu, P. Wang, H. Che, W. Liu, C. Tang, Y. Ao, Triggering dual two-electron pathway for H_2O_2 generation by multiple [Bi-O]n interlayers in ultrathin $Bi_{12}O_{17}Cl_2$ towards efficient piezo-self-Fenton catalysis, Angew. Chem. Int. Ed. 63 (2024) e202316410.
[33] J. Xu, Q. Zhang, X. Gao, P. Wang, H. Che, C. Tang, Y. Ao, Highly efficient Fe^{III}-initiated self-cycled fenton system in piezo-catalytic process for organic pollutants degradation, Angew. Chem. Int. Ed. 62 (2023) e202307018.
[34] D. Sundar, C. Liu, S. Anandan, J. Wu, Photocatalytic CO_2 conversion into solar fuels using carbon-based materials-a review, Molecules 28 (2023) 5383.
[35] Q. Zhang, J. Chen, X. Gao, H. Che, P. Wang, Y. Ao, In-depth insight into the mechanism on photocatalytic synergistic removal of antibiotics and Cr (VI): the decisive effect of antibiotic molecular structure, Appl. Catal. B Environ. 313 (2022) 121443.
[36] Y. Wu, H. Che, B. Liu, Y. Ao, Promising materials for photocatalysis-self-fenton system: properties, modifications, and applications, Small Struct. 4 (2023) 2200371.
[37] Z. Hu, W. Liu, Conversion of biomasses and copper into catalysts for photocatalytic CO_2 reduction, ACS Appl. Mater. Interfaces 12 (2020) 51366–51373.
[38] M. Chen, S. Wang, H. Zhang, P. Zhang, Z. Tian, M. Lu, X. Xie, L. Huang, W. Huang, Intrinsic defects in biomass-derived carbons facilitate electroreduction of CO_2, Nano Res. 13 (2020) 729–735.
[39] X. La, J. Ren, M. Wen, X. Meng, J. Wang, J. Jiang, A. Ragauskas, Microwave resonance enhanced CO_2 reduction using biochar, Environ. Chem. Lett. 6 (1) (2023).
[40] K. Wang, J. Chen, T. Wang, J. Hong, P. Zhao, E. Anthony, Catalytic calcium-looping gasification of biochar with in situ CO_2 utilization with improved energy efficiency, Chem. Eng. J. 472 (2023) 144857.
[41] S. Fu, M. Li, W. de Jong, R. Kortlever, Tuning the properties of N-doped biochar for selective CO_2 electroreduction to CO, ACS Catal. 13 (2023) 10309–10323.
[42] F. Adib, A. Bagreev, T. Bandosz, Analysis of the relationship between H_2S removal capacity and surface properties of unimpregnated activated carbons, Environ. Sci. Technol. 34 (2000) 686–692.
[43] Y. Huang, H. Hu, The interaction of perrhenate and acidic/basic oxygen-containing groups on biochar surface: a DFT study, Chem. Eng. J. 381 (2020) 122647.
[44] B. Delley, From molecules to solids with the $DMol_3$ approach, J. Chem. Phys. 113 (2000) 7756–7764.
[45] J. Perdew, K. Burke, M. Ernzerhof, Generalized gradient approximation made simple, Phys. Rev. Lett. 77 (1996) 3865.
[46] A. Tkatchenko, M. Scheffler, Accurate molecular van der Waals interactions from ground-state electron density and free-atom reference data, Phys. Rev. Lett. 102 (2009) 073005.
[47] J. Wang, J. Fu, Z. Zhao, L. Bing, F. Xi, F. Wang, J. Dong, S. Wang, G. Lin, Y. Yin, Q. Hu, Benefit analysis of multi-approach biomass energy utilization toward carbon neutrality, Innovation 4 (2023) 100423.
[48] Z. E, J. Liang, P. Li, S. Qiang, Q. Fan, A review on photocatalytic attribution and process of pyrolytic biochar in environment, Water Res. 251 (2024), 120994.
[49] A. Gutierrez-Gomez, A. Gallego, R. Palacios-Bereche, J. Leite, A. Neto, Energy recovery potential from Brazilian municipal solid waste via combustion process based on its thermochemical characterization, Energy Fuels 26 (2012) 6366–6386.
[50] F. Mukome, X. Zhang, L. Silva, J. Six, S. Parikh, Use of chemical and physical characteristics to investigate trends in biochar feedstocks, J. Agric. Food Chem. 61 (2013) 2196–2204.
[51] K. Krahn, G. Cornelissen, G. Castro, H. Arp, A. Asimakopoulos, R. Wolf, R. Holmstad, A. Zimmerman, E. Sørmo, Sewage sludge biochars as effective PFAS-sorbents, J. Hazard. Mater. 445 (2023) 130449.
[52] Y. Pan, Y. You, S. Xin, Y. Li, G. Fu, Z. Cui, Y. Men, F. Cao, S. Yu, J. Goodenough, Photocatalytic CO_2 reduction by carbon-coated indium-oxide nanobelts, J. Am. Chem. Soc. 139 (2017) 4123–4129.
[53] M. Keiluweit, P. Nico, M. Johnson, M. Kleber, Dynamic molecular structure of plant biomass-derived black carbon (biochar), Environ. Sci. Technol. 44 (2010) 1247–1253.
[54] H. Yuan, L. Ding, E. Zama, P. Liu, W. Hozzein, Y. Zhu, Biochar modulates methanogenesis through electron syntrophy of microorganisms with ethanol as a substrate, Environ. Sci. Technol. 52 (2018) 12198–12207.
[55] W. Ren, L. Xiong, G. Nie, H. Zhang, X. Duan, S. Wang, Insights into the electron-transfer regime of peroxydisulfate activation on carbon nanotubes: the role of oxygen functional groups, Environ. Sci. Technol. 54 (2020) 1267–1275.
[56] D. Zhong, Y. Jiang, Z. Zhao, L. Wang, J. Chen, S. Ren, Z. Liu, Y. Zhang, D. Tsang, J. Crittenden, pH dependence of arsenic oxidation by rice-husk-derived biochar: roles of redox-active moieties, Environ. Sci. Technol. 53 (2019) 9034–9044.
[57] S. Barman, A. Singh, F. Rahimi, T. Maji, Metal-free catalysis: a redox-active donor-acceptor conjugated microporous polymer for selective visible-light-driven CO_2 reduction to CH_4, J. Am. Chem. Soc. 143 (2021) 16284–16292.
[58] S. Suganuma, K. Nakajima, M. Kitano, D. Yamaguchi, H. Kato, S. Hayashi, M. Hara, Hydrolysis of cellulose by amorphous carbon bearing SO_3H, COOH, and OH groups, J. Am. Chem. Soc. 130 (2008) 12787–12793.
[59] J. Sheng, Y. He, J. Li, C. Yuan, H. Huang, S. Wang, Y. Sun, Z. Wang, F. Dong, Identification of halogen-associated active sites on bismuth-based perovskite quantum dots for efficient and selective CO_2-to-CO photoreduction, ACS Nano 14 (2020) 13103–13114.
[60] J. Feng, C. Mak, L. Yu, B. Han, H. Shen, S. Santoso, M. Yuan, F. Li, H. Song, J. Colmenares, H. Hsu, Structural modification strategies, interfacial charge-carrier dynamics, and solar energy conversion applications of organic-inorganic halide perovskite photocatalysts, Small Methods (2023) 2300429.
[61] C. Huang, B. Mohamed, L. Li, Comparative life-cycle assessment of pyrolysis processes for producing bio-oil, biochar, and activated carbon from sewage sludge, Resour. Conserv. Recycl. 181 (2022) 106273.